CLIMATE CHANGE AT THE PALEOCENE-EOCENE BOUNDARY: NEW INSIGHTS FROM MOLLUSKS AND ORGANIC CARBON IN THE HANNA BASIN OF WYOMING

Pennilyn Higgins[*]

[*] Department of Earth and Environmental Sciences, University of Rochester, Rochester, NY 14627, loligo@earth.rochester.edu

ABSTRACT

Climate change at the Paleocene-Eocene Thermal Maximum (PETM) is frequently regarded as among the best ancient proxies for the potential effects of modern climate change. Terrestrial sections recording this event are few, but essential in understanding the impacts of rapid global change on land-dwelling life forms such as humans. In the Hanna Formation, exposed in the Hanna Basin of south-central Wyoming, the PETM and associated climate change are recorded in lacustrine and fluvial sediments bracketing the Paleocene-Eocene boundary. Isotopic analysis of abundant fossil mollusks and organic carbon reveal interesting trends in the warming during the PETM and the subsequent climatic recovery. Changes in sedimentary environment due to climate change or tectonic events may be distinguishable through isotopic study, helping to clarify the direct impact of climate change on terrestrial ecosystems.

Introduction

Rapid global changes in climate (warming or cooling) are usually associated faunal turnover and frequently define the boundaries between adjacent geochronologic units. The Paleocene-Eocene boundary (~55Ma) is associated with an episode of global warming, termed the Paleocene-Eocene Thermal Maximum (PETM). In Wyoming, mean annual temperature estimated from fossil floras increased from about 10°C at the end of the Paleocene to 20–25°C in the early Eocene (Koch *et al.*, 2003). This warming event corresponds with changes in the marine realm including the extinction of benthic foraminifera and a decrease in the surface-to-bottom water thermal gradient in the oceans (Koch *et al.*, 1992; 2003), as well as mammalian turnover such as the first appearance of ungulate groups and euprimates (Gingerich, 2003; Koch *et al.*, 2003). Warming associated with the PETM is thought to have reached its maximum in about 50ky (Kennett & Stott, 1991; Zachos *et al.*, 1993; Röhl *et al.*, 2000; Koch *et al.*, 2003), then gradually returned to pre-PETM conditions over about 170ky (Kennett & Stott, 1991; Dickens *et al.*, 1997; Bains *et al.*, 2003; Koch *et al.*, 2003; Röhl *et al.*, 2007) although recent research suggests that the PETM may have ended as abruptly as it began (Bowen & Zachos, 2010).

Global warming and the CIE during the PETM has been attributed most frequently to an increase in atmospheric carbon dioxide due to the release of methane hydrates from ocean basins (Dickens *et al.*, 1995; 1997; Bains *et al.*, 1999). However, there is debate about whether the release of methane hydrates alone could be responsible for the rapid climate change and CIE at the beginning of the Eocene (Kvenvolden, 1999). Other potential sources of carbon dioxide that could result in global warming and the negative carbon isotope excursion involve the burning of large amounts of sedimentary organic carbon due to complete combustion of Paleocene peatlands, emplacement of large igneous provinces into organic-rich sediments, or the isolation and subsequent desiccation of a large epicontinental seaway (Higgins & Schrag, 2006).

The inception of the PETM is recognized globally by a negative carbon isotope excursion (CIE), during which the $\delta^{13}C$ values in terrestrial carbonaceous materials exhibit a ~2.8-8‰ de-

crease (Koch *et al.*, 1992; Koch *et al.*, 2003; Magioncalda *et al.*, 2004) and marine carbonaceous materials exhibit a −2.5‰ decrease (Bains *et al.*, 2003). In terrestrial organic carbon (coal or carbonaceous shale), $\delta^{13}C$ values more negative than −26‰ V-PDB are found in rock representing the CIE, whereas values around −25‰ represent background pre- and post-PETM values (Harrington *et al.*, 2005). The CIE is also recognized in paleosol carbonate nodules when values fall below about −12‰ V-PDB (Bains *et al.*, 2003; Magioncalda *et al.*, 2004). Furthermore, the CIE is recognized in marine carbonaceous sediments when $\delta^{13}C$ values fall below 2‰ V-PDB (Bains *et al.*, 1999). Fossil mollusk shells and fossil mammal teeth also provide records of the CIE (Schmitz & Andreasson, 2001; Koch *et al.*, 2003; Ivany *et al.*, 2004).

Several terrestrial Paleocene–Eocene boundary sections are known from the western interior of North America. These include sections in the Williston Basin, North Dakota, (Harrington, 2004; Harrington *et al.*, 2005), Green River Basin, Wyoming (Fricke & Wing, 2004), and the Powder River Basin, Wyoming (Wing *et al.*, 2003; Harrington, 2003; 2004). The most widely studied of these sections are in the Bighorn and Clarks Fork basins of northwestern Wyoming (Koch *et al.*, 1995; Clyde & Gingerich, 1998; Gingerich, 2001; Bains *et al.*, 2003; Koch *et al.*, 2003; Harrington, 2003; Gingerich, 2003; Magioncalda *et al.*, 2004; Fricke & Wing, 2004; Harrington, 2004; Clyde *et al.*, 2005; Kraus & Riggins, 2007; Yans *et al.*, 2006; Smith *et al.*, 2007), where the CIE observed from abundant paleosol carbonates, organic carbon, and mammalian fossils has been used to correlate terrestrial PETM sections to marine records of the PETM (Bains *et al.*, 2003; Magioncalda *et al.*, 2004) and to North American Land Mammal "Ages" (Koch *et al.*, 1995; Gingerich, 2003). The present study introduces a new terrestrial PETM section from the Hanna Basin of south-central Wyoming, which contains an expanded, highly organic section of rock known to bracket the PETM.

The Paleocene-Eocene boundary in the Hanna Basin

The Hanna Basin is a small but complex structural basin in south-central Wyoming (figure 1) that formed during the deformation of the Laramide Orogeny (Late Cretaceous through
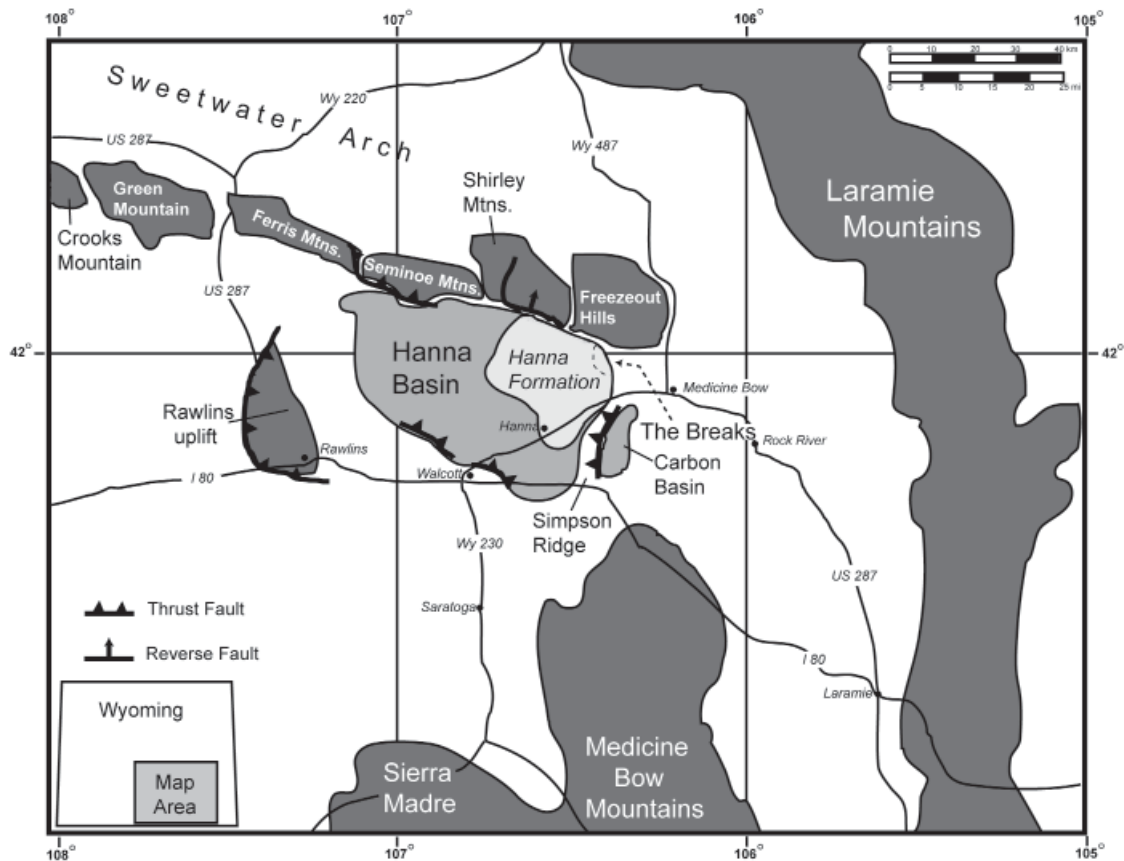
Figure 1. Location map showing the position of the Hanna Basin within Wyoming, and of The Breaks within the Hanna Basin.

early Eocene; Lillegraven & Snoke, 1996; Lillegraven & Eberle, 1999; Higgins, 2003; Lillegraven *et al.*, 2004). It contains nearly 13 km of sediments, with all but about one km representing deposits of Cretaceous through early Eocene age (Lillegraven & Snoke, 1996; Higgins, 2003). The three-kilometer thick Hanna Formation is exposed in the northeastern corner of the Hanna Basin, in an area of badlands called "The Breaks" (figure 1). This thick package of terrestrial sediments (figure 2) deposited from late-early Paleocene (Torrejonian North American Land Mammal "Age" or NALMA) through the earliest Eocene (Wasatchian NALMA) is the result of uplift and erosion of mountains of the Sweetwater Arch during the peak of local Laramide tectonism (Lillegraven & Snoke, 1996; Higgins, 2003; Lillegraven *et al.*, 2004). The Hanna Formation is composed dominantly of organic-rich floodplain and fine-grained alluvial fan deposits with two distinct units of lacustrine deposits, termed the upper lacustrine unit (ULU) and the lower lacustrine unit (LLU), that are each 300–400 meters thick in the upper half of the Hanna Formation. The upper half of

the Hanna Formation also contains numerous numbered coal beds that are currently actively mined (figure 2; Dobbin *et al.*, 1929; Lillegraven *et al.*, 2004).

On the basis of mammalian and molluscan biostratigraphy and palynology, the Paleocene-Eocene boundary is believed to lie somewhere between 2000m and 3000m above the base of the Hanna Formation in The Breaks (Kirschner 1984; Lillegraven & Snoke, 1996; Higgins, 2003; Dunn, 2003; Lillegraven *et al.*, 2004; figure 2). This interval includes both the upper and the lower lacustrine units and about 300m of intervening fine-grained fluvial and paludal strata. This relevant part of the Hanna Formation starts at coal 78 and continues through coal 89 of Dobbin *et al.* (1929). Through focused efforts on this part of the Hanna Formation, three objectives are planned with this research:

1) Identify the probable position of the onset of the CIE (and thus the PETM), through isotopic analysis of dispersed organic carbon (DOC);

2) To identify millennial-scale environmental changes that occurred during the PETM using
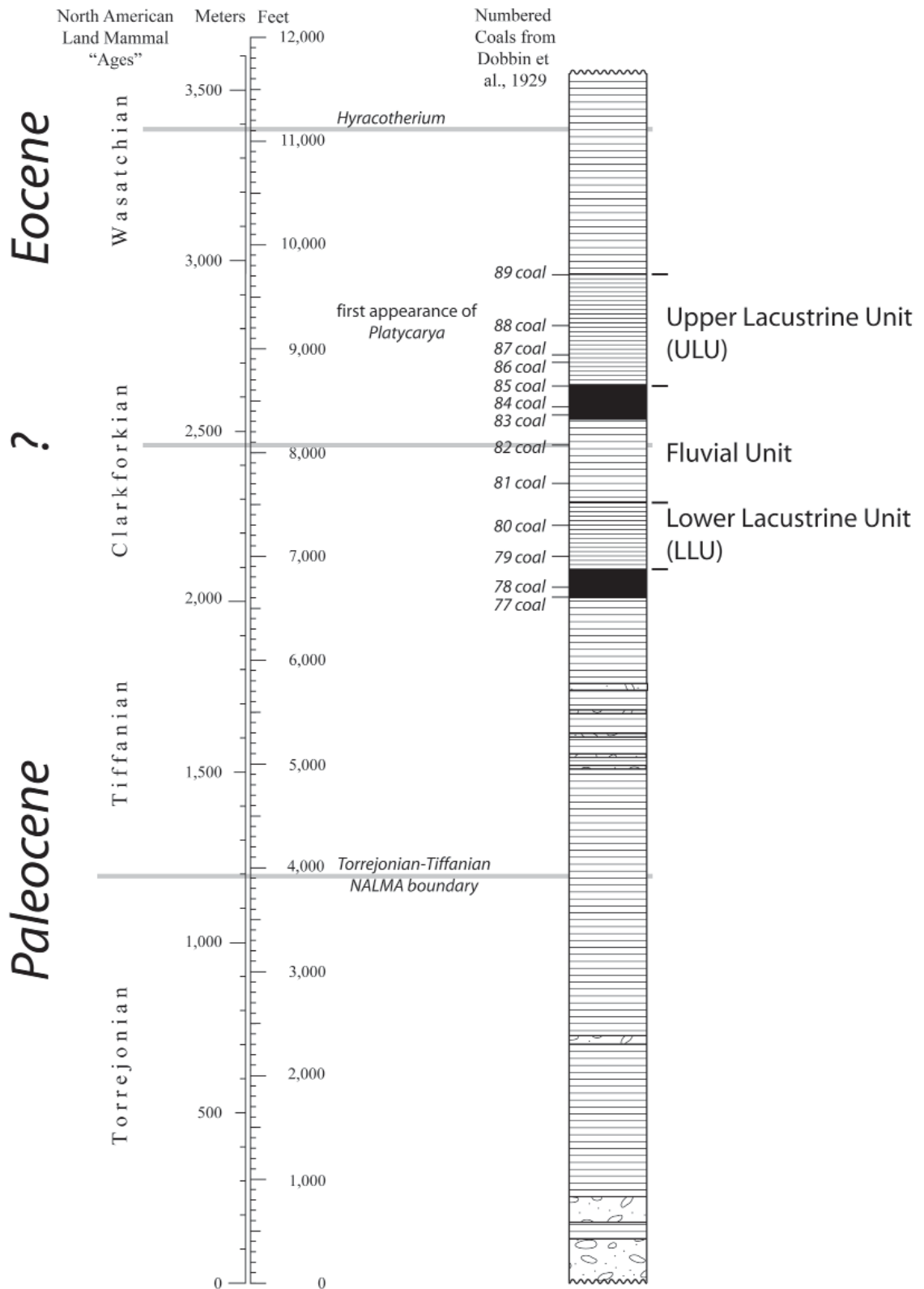
Figure 2. Composite section of the Hanna Formation in the vicinity of The Breaks. Important stratigraphic markers and the location of the section studied for this analysis are highlighted. Modified from Lillegraven *et al.* (2004).

the isotopic composition of nitrogen, where nitrogen is sufficiently abundant to yield an adequate result;

3) To examine intra-annual changes in environment using serial isotopic analysis of carbonate from the abundant shells of lacustrine mussels in the upper and lower lacustine units.

Methods

In 2007, approximately 1000 meters of the Hanna Formation were measured, beginning at the base of the lower lacustrine unit and continuing to the top of the upper lacustrine unit and coal 89 (figure 2). During measurement, organic-rich rock and coal samples were collected as well as freshwater mollusk fossils as they were recognized. In 2009, an additional section, parallel to the first but about one km north, spanning from the top of the lower lacustrine unit into the middle of the upper lacustine unit was also measured, and numerous additional samples were collected.

Carbon and nitrogen isotopic ratios of dispersed organic matter were measured from the rock and coal samples. All samples were powdered then pretreated with ˜ 12% hydrochloric acid to remove any secondary carbonates. Powders were enclosed in tin capsules and analyzed using a Costech Analytical 1040ES elemental analyzer attached to a ThermoFinnigan Delta Plus XP mass spectrometer in the Department of Earth and Environmental Sciences at the University of Rochester. Carbon and nitrogen isotopic results are reported using the standard delta notation in ‰ relative to V-PDB (Vienna Pee-Dee Belemnite) for carbon and air for nitrogen and normalized (Coplen, 1994) on scales such that the carbon isotopic values of SRM 8541 (Graphite), SRM 8542 (Sucrose), and SRM 8530 (Oil) are −15.9‰, −10.47‰, and −19.73‰, respectively and the nitrogen isotopic values of SRM 8558 and 8459 (both KNO3) are 179.9‰ and 3.5‰ respectively.

Both gastropods and pelecypods were collected for intrashell stable isotopic analysis to look at paleoenvironemental changes (Romanek & Grossman, 1989; Andreasson & Schmitz, 1996; Dettman *et al.*, 1999; Schmitz & Andreasson, 2001; Jones *et al.*, 2002; Goodwin *et al.*, 2003; Ivany *et al.*, 2004; Goodwin *et al.*, 2004; Schöne *et al.*, 2006). Fourier-Transform Infrared Spectroscopy (FT-IR) was used on several fossil

shells to assess the state of diagenetic alteration (Vagenas *et al.*, 2003). Six shells were selected for serial isotopic analysis, representing five fossiliferous levels within the CIE, spanning nearly 600 m of section within the Hanna Formation. Isotope samples were collected using a dental drill and tracing growth bands on the surface of the shell (figure 3) without penetrating deeply into the shell.

Shell samples were analyzed using ThermoFinnigan Gas Bench attached to the ThermoFinnigan Delta Plus XP mass spectrometer in continuous flow mode in the Department of Earth and Environmental Sciences at the University of Rochester. Approximately 200ffig of sample is needed for each analysis. Samples were reacted with 103% phosphoric acid at a temperature of 69℃ for at least 0.5 hour to as long as 7 hours. Carbon and oxygen isotopic results are reported using the standard delta notation in ‰ relative to VPDB (Vienna Pee-Dee Belemnite) and normalized (Coplen, 1994) on scales such that the carbon and oxygen isotopic values of NBS-19 are 1.95‰ and −2.2‰, respectively, carbon and oxygen isotopic values of NBS-18 are −5.01‰ and −23‰, respectively, and the carbon isotopic value of L-SVEC is −46.6‰.

Results and Discussion

Carbon Isotope Excursion

A composite stratigraphic column of the part of the Hanna Formation measured for this study is shown in figure 4. Isotopic results from analysis of organic samples are shown on this plot. Mean δ^{13}C values and standard deviations of replicate analyses are provided in table 1.
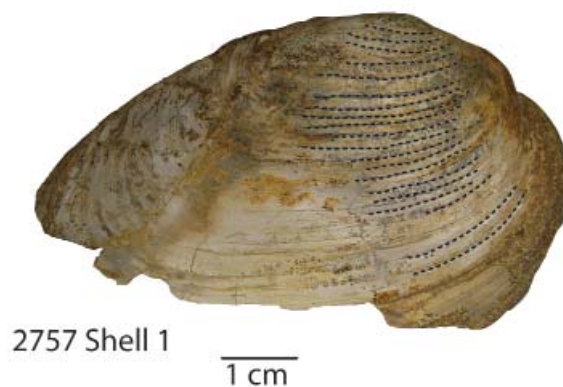

2757 Shell 1
1 cm

Figure 3. Bivalve shell TB 2757-1 from 2757m level. Dashed lines indicate sampling grooves. Photography by the author.
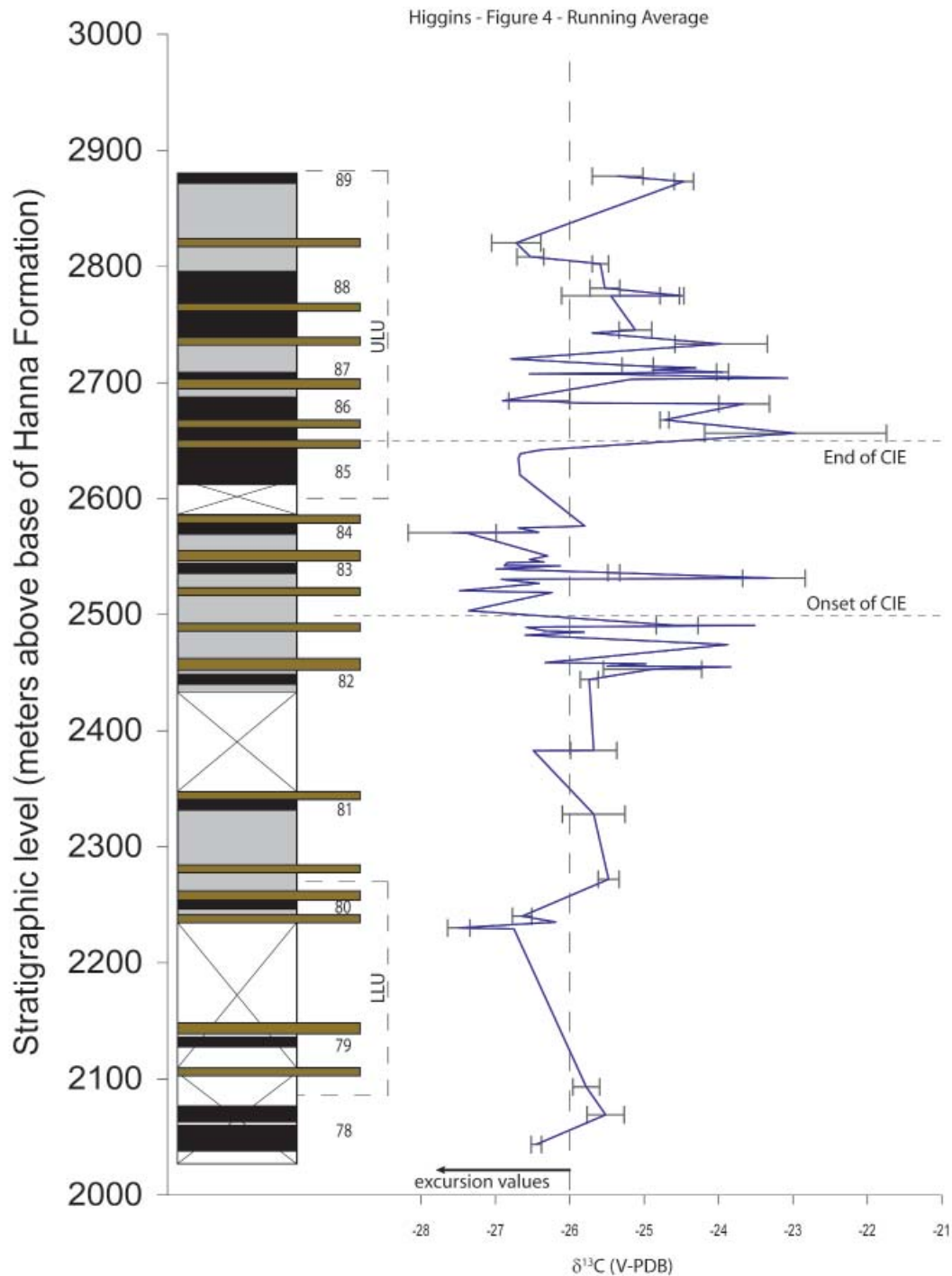
Figure 4. Organic carbon isotope stratigraphy across the Paleocene-Eocene boundary in the Hanna Formation. Error bars indicate standard deviations of replicate analyses.

The overall pattern is quite noisy, with frequent but reproducible fluctuations of as much as two or three permil between sampling localities. The onset of the CIE is recognized by the drop in carbon isotopic values from as positive as −23.8‰ at around 2455m to −27.4‰ at about 2504m, with isotopic values first consistently below −26‰ at 2483m. Isotopic values more negative than −26‰ are considered typical for the CIE (Magioncalda *et al.*, 2004; Harrington *et al.*, 2005). This negative excursion continues to about 2657m where values return to values consistently more positive that −26‰. The whole of the presumed CIE includes at least two spikes back to more positive values, one at 2491m (−23.5‰) and one at 2532m (−23.3‰).

The variability in values from Hanna Formation may be due to short-term perturbations in

Sample	δ¹³C	Standard Deviation of Replicate Analyses	Mass Fraction Carbon	Strati-graphic Level (m)	Sample	δ¹³C	Standard Deviation of Replicate Analyses	Mass Fraction Carbon	Strati-graphic Level (m)
PH-TB-07-97	-25.4	0.34	29.9	2878	PH-TB-07-97	-25.4	0.34	29.9	2878
PH-TB-07-96	-24.8	0.13	55.8	2873.5	PH-TB-09-48	-26.3		13.7	2545.5
PH-TB-07-94	-26.7	0.33	20.5	2820.5	PH-TB-09-47	-26.8		9.2	2545.0
PH-TB-07-92	-26.5	0.18	21.7	2808.5	PH-TB-09-18	-26.9		4.1	2542.5
PH-TB-07-91	-25.6	0.11	11.6	2802.5	PH-TB-09-46	-26.1		6.0	2542.3
PH-TB-07-89	-25.5	0.20	31.0	2781.5	PH-TB-09-17	-27.0		28.7	2539.4
PH-TB-07-88	-25.4	0.66	36.6	2775	PH-TB-07-20	-25.4	0.08	10.3	2536.3
PH-TB-07-90	-24.5	0.03	34.5	2775	PH-TB-09-16	-23.3	0.42	31.5	2531.7
PH-TB-07-87	-25.1	0.22	31.0	2745.5	PH-TB-09-15	-26.9		2.7	2530.7
PH-TB-09-33	-24.0	0.62	42.6	2733.5	PH-TB-09-14	-26.4		32.2	2527.1
PH-TB-07-86	-26.8		6.5	2720.5	PH-TB-09-45	-27.5		27.7	2520.8
PH-TB-07-85	-25.1	0.21	9.1	2714.5	PH-TB-09-13	-26.2		18.1	2519.3
PH-TB-09-31	-24.3		8.3	2712.8	PH-TB-09-43	-27.4		3.6	2503.5
PH-TB-09-30	-24.9		17.4	2711.3	PH-TB-09-12	-24.6	0.28	15.7	2490.9
PH-TB-09-29	-23.9	0.08	40.6	2709.2	PH-TB-09-42	-23.5		25.8	2490.9
PH-TB-09-75	-26.5		6.4	2707.6	PH-TB-09-41	-26.6		2.2	2489.3
PH-TB-09-28	-25.3		10.0	2707.2	PH-TB-09-40	-26.3		3.2	2486.2
PH-TB-09-27	-23.1		55.7	2704.1	PH-TB-09-10	-25.8		15.2	2485.3
PH-TB-09-26	-25.2		6.4	2703.0	PH-TB-09-09	-26.1		9.5	2484.2
PH-TB-09-69	-26.9			2684.6	PH-TB-09-38	-26.6		3.4	2482.5
PH-TB-07-46	-26.4	0.41	25.8	2684.3	PH-TB-09-08	-23.9		62.8	2474.4
PH-TB-09-68	-25.9		11.2	2682.5	PH-TB-09-07	-26.3		2.3	2458.9
PH-TB-07-44	-23.7	0.34	85.1	2681.8	PH-TB-09-36	-25.0		11.3	2457.9
PH-TB-07-84	-24.7	0.06	9.9	2668.0	PH-TB-09-06	-25.5		16.8	2455.8
PH-TB-07-83	-23.0	1.22	59.4	2656.5	PH-TB-09-35	-23.8		49.8	2455.2
PH-TB-09-66	-26.4			2642.1	PH-TB-09-34	-24.9	0.66	5.6	2453.1
PH-TB-09-65	-26.7		7.7	2638.9	PH-TB-07-18	-25.7	0.12	6.8	2444.3
PH-TB-07-41	-26.7		9.9	2635.3	PH-TB-07-30	-25.7	0.31	48.9	2383.3
PH-TB-09-60	-26.7			2620.5	PH-TB-09-03	-26.5		11.4	2383.1
PH-TB-09-54	-25.8		49.1	2576.4	PH-TB-07-26	-25.7	0.42	17.3	2328.3
PH-TB-09-53	-26.7		15.0	2574.9	PH-TB-07-22	-25.5	0.14	40.8	2272.3
PH-TB-09-52	-26.4		8.4	2571.2	PH-TB-07-10	-26.6	0.13	13.0	2240.3
PH-TB-07-35	-27.6	0.59	10.9	2570.8	PH-TB-07-12	-27.5	0.15	13.3	2230.3
PH-TB-09-51	-27.4		18.3	2570.2	PH-TB-07-05	-25.8	0.18	19.9	2093.3
PH-TB-09-19	-26.3		12.9	2550.8	PH-TB-07-04	-25.5	0.25	11.0	2069.3
PH-TB-09-50	-26.5		17.0	2547.6					

Table 1. Means and standard deviations of isotopes of organic carbon by stratigraphic level.

environmental conditions which are evident due to the great thickness of the CIE, at about 150 m (figure 4), compared with a similar section in the Bighorn Basin of Wyoming where the CIE is only about 40 m thick (Bains *et al.*, 2003; Magioncalda *et al.*, 2004). Additionally, the noise may be due the selection of bits of coal from the Hanna Formation for isotopic analysis, rather than grinding whole rocks for bulk analysis. Various sources of carbon measured in analyses of bulk organic carbon (leaves, roots, stems, seeds) may all differ substantially from one another even if from the same plant (Schouten *et al.*, 2007; Smith *et al.*, 2007; Bechtel *et al.*, 2008; Carvajel-Ortiz *et al.*, 2009). Magioncalda *et al.* (2004) argue that these various signals are typically averaged in dispersed organic carbon, resulting in a reliable pattern which is comparable with other carbon isotopic records from different regions or different substrates. Several samples from the Hanna Formation, however, are selected pieces of coalified wood or leaves, rather than bulk mixtures of dispersed organic carbon, which could increase the variability of isotopic results throughout the section and even from single localities.

A three-point running average was applied to the carbon isotopic data from the Hanna Formation to minimize this noise, and this was compared directly to the organic carbon data at Polecat Bench (figure 5). The isotope stratigraphy is aligned based upon the hypothesized onset and end of the CIE in the Hanna Formation (discussed above), and the onset and end of the CIE as defined by Magioncalda *et al.* (2004) for organic carbon at Polecat Bench. The overall match of the patterns is remarkable, especially at the positive excursion at about 2935 m in the Hanna Formation and the negative excursions at 2520 and 2845 m.

Magioncalda *et al.* (2004) noted that the onset of the CIE as identified from isotopic analysis of organic carbon was delayed by about 3-5 m from the onset of the CIE recognized from the analysis of paleosol carbonates by Bains *et al.* (2003). Magioncalda *et al.* (2004) hypothesized that the difference lies in the fact that paleosol carbonates do form in the subsurface and the atmospheric carbon dioxide likely circulated to depths at which the carbonate nodules formed. Organic carbon was deposited near the surface, resulting in the separation between the CIE in organic carbon and in paleosol carbonate nod-

ules. Based upon this, the Paleocene-Eocene boundary, marked by the onset of the CIE in paleosol carbonate nodules is about 5 meters below the onset of the CIE in organic carbon (and is noted in figure 5). Using only the onset of the CIE in the Hanna Formation, the Paleocene-Eocene boundary lies at approximately 2500 m. Paleosols with obvious carbonate nodules are not present in the Hanna Formation to allow further exploration of the relationship between the onset of the CIE if measured using organic carbon or carbonate carbon.

Nitrogen
The abundance of nitrogen in organic matter is significantly lower than that of carbon. Nitrogen isotopes and C/N ratios are usually not measured for samples of ancient organic carbon because the relative abundance of nitrogen is too low for accurate measurement. However, because of the high abundance of organic material in coals in the Hanna Formation, some measurements were made successfully.

A common measure used when examining nitrogen in sediments in the carbon to nitrogen atomic ratio (C/N atomic). This ratio is variable, based upon the origin of the nitrogen-bearing organic molecules. Where most of the organic material is derived from algal matter, C/N ratios are typically less than 10 (Meyers & Ishiwatari, 1993; Meyers, 1997; Bertrand *et al.*, 2004; Routh *et al.*, 2004; Choudhary *et al.*, 2009). Whereas, if the bulk of organic matter is derived from vascular plants (typically terrestrial), C/N ratios are greater than 20 (Meyers & Ishiwatari, 1993; Choudhary *et al.*, 2009). Diagenetic degradation of organic matter is thought to reduce this ratio (Meyers & Ishiwatari, 1993), but the reduction is not so extreme to cause terrestrially derived organic matter to have the C/N rato of algally derived organic matter. Figure 6 and table 2 show C/N ratios from 14 samples from the Hanna Formation with sufficient nitrogen for analysis. C/N ratios average about 42, which is fully in the range of land-derived organic carbon. There is a slight trend from higher C/N ratios (maximum of 66 at 2455 m) to lower ratios (minimum of 27 at 2878 m), which a potential shift from most carbon coming from land plants to a greater influence of algal sources of organic matter (Meyers & Ishiwatari, 1993; Meyers, 1997).
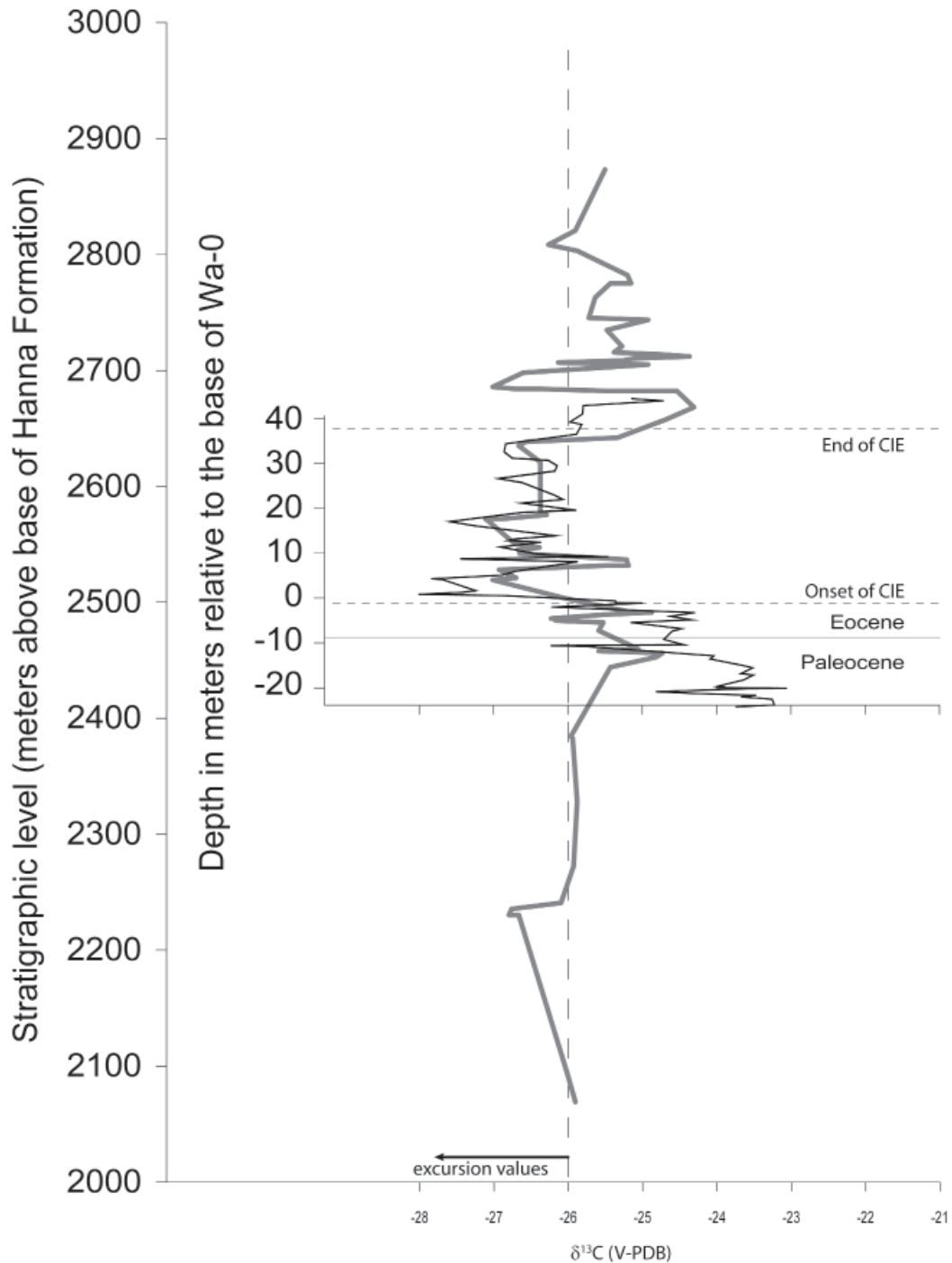
Figure 5. Three-point running average of the organic carbon isotope stratigraphy in the Hanna Formation overlain by the organic carbon isotope stratigraphy of Magioncalda *et al.* (2004).

Isotopes of nitrogen provide additional insight into the origin of organic matter in a lake system and may provide some information about the general environmental status of lake environments (Meyers & Ishiwatari, 1993; Yamamuro & Kanai, 2005; Choudhary *et al.*, 2009). Importantly, the most negative natural values of $\delta^{15}N$ are typically about −1 to 3‰ representing the activity of cyanobacteria. Land

plants overlap this with values from 1 to 3.7‰ (Meyers & Ishiwatari, 1993). Values of 8‰ or greater are characteristic of phytoplankton (Meyers & Ishiwatari, 1993), but could potentially be much lower and overlap that of cyanobacteria (Choudhary *et al.*, 2009).

Most measured $\delta^{15}N$ values from the Hanna Formation lie in the −1 to 3‰ range, indicating either presence of cyanobacteria or a domi-
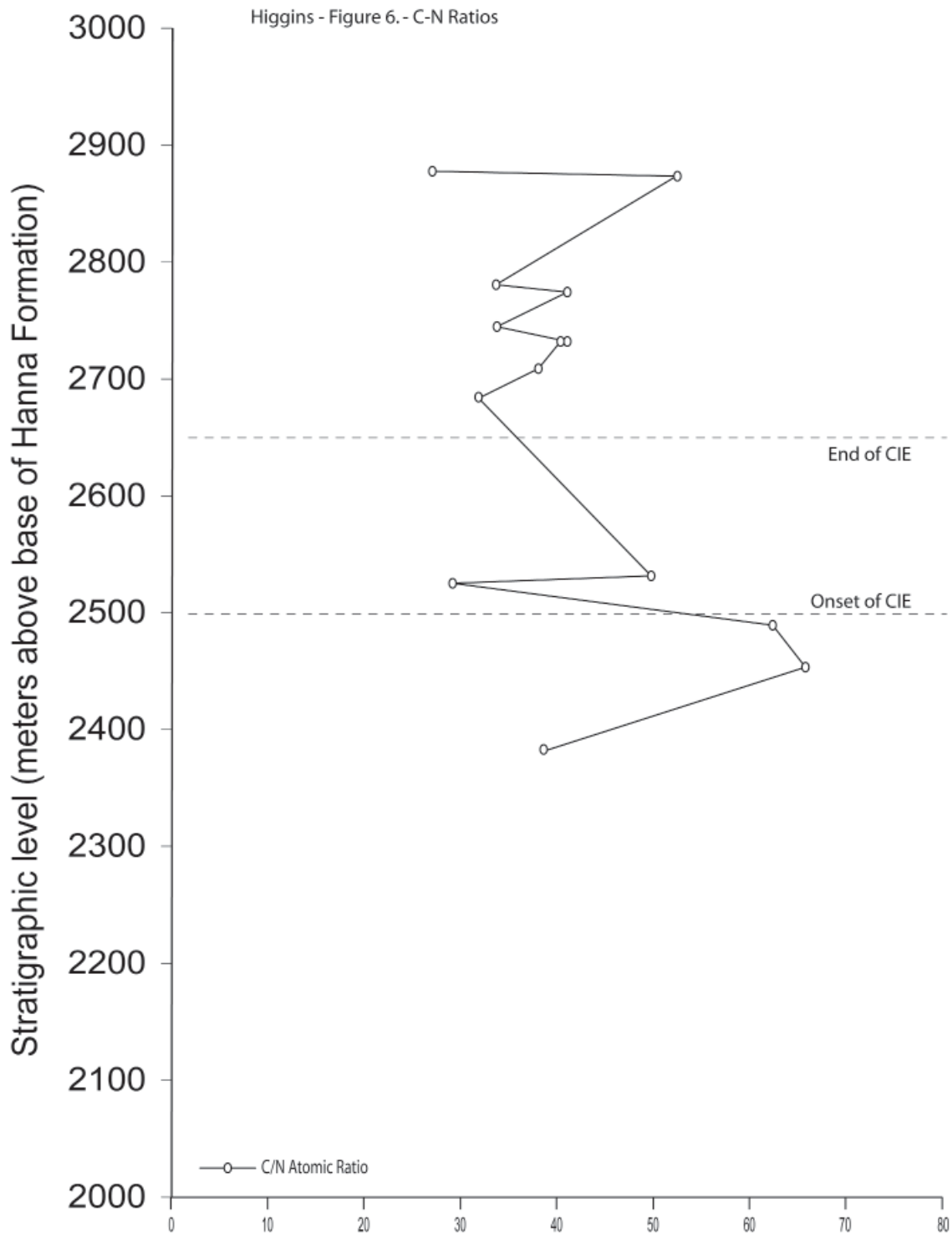
Figure 6. Carbon to nitrogen ratios for samples in the Hanna Formation for which carbon and nitrogen abundances and isotopic ratios were measured (table 2).

nance of land plants (figure 7). C/N ratios do not support the former (Meyers & Ishiwatari, 1993; Choudhary *et al.*, 2009), thus land plants appear to dominate the source of organic material in the Hanna Formation. There are notable exceptions to this overall pattern, however. At about 2455, 2710, 2875, and most extremely at 2685 meters, $\delta^{15}N$ values are far more negative than expected for typical modern lacustrine systems. The value of −10.8‰ at 2684 meters is highly suspect and is likely an analytical anomaly and will not be considered further. In the others,

Sample ID	δ¹³C (V-PDB)	δ¹⁵N (AIR)	Weight % Carbon	Weight % Nitrogen	C/N atomic	Stratigraphic level
PH-TB-07-97	-25.4	-0.8	48.9	1.3	27.1	2878.0
PH-TB-07-96	-24.5	-1.8	49.8	1.2	52.5	2873.5
PH-TB-07-89	-25.5	0.0	51.3	1.1	33.7	2781.5
PH-TB-07-88	-25.5	1.4	32.2	1.0	41.1	2775.0
PH-TB-07-87	-25.1	-0.8	48.7	1.1	33.8	2745.5
PH-TB-09-33	-24.0	1.0	25.8	1.4	40.4	2733.5
PH-TB-09-33	-24.0	2.5	42.7	1.4	41.1	2733.5
PH-TB-09-29	-24.0	-1.9	47.6	1.3	38.1	2709.2
PH-TB-07-46	-26.4	-10.8	47.6	0.9	31.9	2684.3
PH-TB-09-16	-23.3	2.8	31.0	1.1	49.9	2531.7
PH-TB-09-14	-26.4	5.5	36.6	1.3	29.2	2527.1
PH-TB-09-12	-24.6	-0.7	31.0	1.0	62.5	2490.9
PH-TB-09-35	-23.8	-3.0	55.8	0.9	65.9	2455.2
PH-TB-07-30	-25.7	-0.1	29.9	1.5	38.7	2383.3

Table 2. Carbond and nitrogen measurements.

$\delta^{15}N$ values are about 1 to 2 ‰ more negative than reported 'typical' values for the organic material left during cyanobacterial activity (Meyers & Ishiwatari, 1993). These negative values may be due to either differences in atmospheric $\delta^{15}N$ at the Paleocene-Eocene boundary (which are unknown at this time) or due to the activity of prolific nitrogen-fixing bacteria at these times (Meyers, 1997).

At about 2530 meters, the lowest datapoint within the CIE, $\delta^{15}N$ becomes more positive than elsewhere (5.5‰). More positive $\delta^{15}N$ values have been attributed to the increased activity of phytoplankton (Meyers & Ishiwatari, 1993; Choudhary *et al.*, 2009), but may also suggest drying of the environment (Meyers & Ishiwatari, 1993). An interpretaion of drying seems reasonable as this stratigraphic level also marks the onset of warming in the early Eocene.

Mussel Isotopes
Stable isotopes in the shells of extant mollusks have been shown to vary according to general climatic regimes, with different environments (*i.e.* temperate *vs.* tropical) having distinctive isotopic signatures (Romanek & Grossman, 1989; Andreasson & Schmitz, 1996; Dettman *et al.*, 1999; Schmitz and Andreasson, 2001; Jones *et al.*, 2002; Goodwin *et al.*, 2003; Ivany *et al.*, 2004; Goodwin *et al.*, 2004; Schöne *et al.*, 2006). Isotopes of oxygen in the shells of mussels are derived from the water in which they lived and usually track seasonal changes in the isotopes of water, which themselves are related to temperature and precipitation. Usually, increased oxygen values are associated with cooler times (winter) and decreased oxygen values are associated with warmer times (summer; Grossman and Ku, 1986; Jones and Quitmeyer, 1996; McConnaughey, 2003; Jones *et al.*, 2005). Carbon isotopes in shells of aquatic mollusks are derived from environmental CO_2 (in the form of dissolved inorganic carbon [DIC]), with some unknown contribution from respired or metabolic carbon (CM). The contribution of CM within the mussels of the Hanna Formation is assumed to be the same for all individuals and to have minor annual variation. Isotopic changes in DIC, however, can experience large seasonal changes related to environmental changes over the course of the year (Jones *et al.*, 2001; Brunet *et al.*, 2009).

Mollusks (both pelecypods and gastropods) are abundant within the two lacustrine units of the Hanna Formation. Five localities with fossil mussels were selected for study. Two sites are found in the lower lacustine unit (LLU), which is late Paleocene in age, having been deposited prior to the onset of the CIE. The remaining three sites occur in the upper lacustrine unit (ULU). One is low in the ULU, and is in the uppermost part of the CIE. The others occur post-CIE. Serial isotopic analysis of mussel shells from these five different levels in the Hanna Formation (Fig. 8) was conducted to explore intra-annual changes in environment prior to, during, and following the CIE.
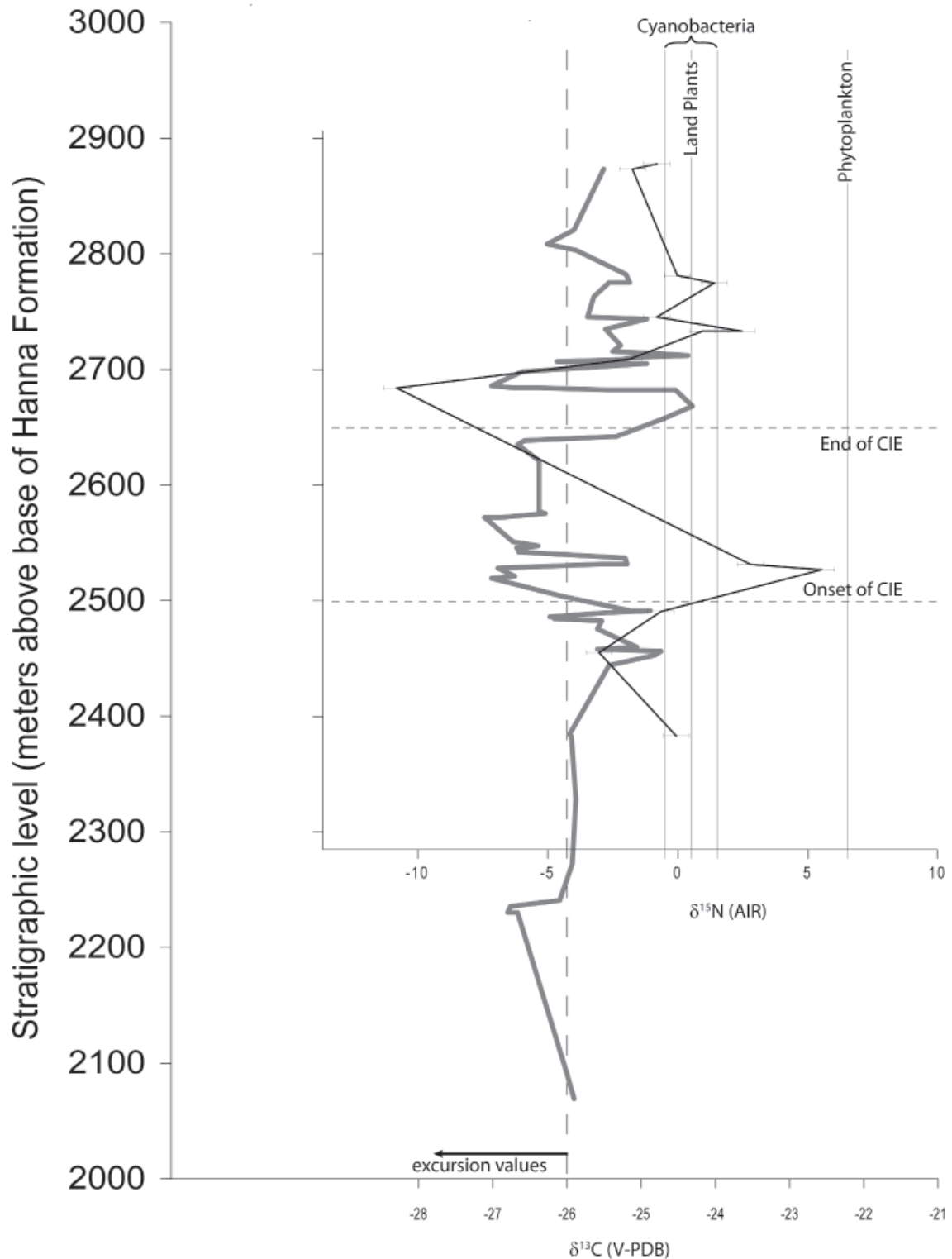
Figure 7. Nitrogen isotope stratigraphy across the Paleocene-Eocene boundary in the Hanna Formation.

FT-IR analysis on four shell collected from the Hanna Formation showed the shells to be composed of aragonite, from which I conclude that diagenetic alteration is minimal. All shells collected for this analysis were relatively complete and showed layering structures that allow confidence that the original shell material is preserved, and that isotopic data collected from shells reflect the original isotopic values.

From the five sites, a total of eight individual shells were sampled. The raw isotopic data are provided in Appendix 1. Statistics for each shell

are provided in table 3. These means are also plotted against stratigraphic level and the organic carbon isotopes on figure 8. Overall, there is little obvious pattern evident in the carbon isotopes, except perhaps a slight increase in the means overall, which seems to track changes in organic carbon isotopic values for each site (figure 8). This may be due to changes in the isotopic value of organic carbon available to the mussels in life, which would be reflected in the small contribution of CM in the shell carbonate (McConnaughey *et al.*, 1997; Gillikin *et al.*, 2006; McConnaughey & Gillikin, 2008). Oxygen isotopes as well show no clear stratigraphic trend (figure 8).

Using variation of oxygen isotopes as a marker for time-of-year, Seasonal environmental changes over the course of the life of the mussel can be correlated to specific times of the year with combined analysis of carbon and oxygen isotopes in fossil mussels. The cyclical pattern of $\delta^{18}O$ values is interpreted as an annual seasonal signal, with peaks of maximum $\delta^{18}O$ occurring in winter and minima in $\delta^{18}O$ representing summer. Where $\delta^{18}O$ and $\delta^{13}C$ in a shell covary with a positive correlation coefficient, productivity (*i.e.* photosynthesis) dominated the aquatic regime during the cooler months and bacterial respiration dominated in the summer (Jones *et al.*, 2001; Brunet *et al.*, 2009). Where $\delta^{13}C$ and $\delta^{18}O$ are inversely correlated (a negative correlation coefficient), productivity increased during the warmer months (Jones *et al.*, 2001; Brunet *et al.*, 2009).

Shells collected throughout the Hanna Formation exhibit a trend from no or weakly negative correlation coefficients in the Paleocene part of the section (in the lower lacustrine unit), to strongly positive correlation coefficients in the upper lacustrine unit above the end of the CIE. This suggests a shift from environments where phytoplankton and land plants dominated the environment in and around the lakes, toward an environment where bacterial respiration dominated the system. This seems more reasonable when one considers the abundance of large stromatolitic structures found throughout the lower and especially the upper lacustrine units. However, the direct relationships between stromatolites and the shell-bearing units is currently unclear, and will be a topic of future research.

Conclusions

Isotopic analyses of organic carbon in the upper parts of the Hanna Formation clearly indicate the CIE associated with the PETM. The overall pattern is very similar to that from organic carbon at Polecat Bench (Magioncalda *et al.*, 2004), but is found within a rock column approximately three times thicker. This represents an unparalleled opportunity to look at the CIE at extremely high resolution in a terrestrial section. One important observation is the recognition of a large, short-lived shift in carbon isotopes back to pre-CIE values.

New data from nitrogen (isotopes and concentration) provide insights into the origins of organic matter into the Hanna Formation. To a large degree, most organic material appears to have been derived from terrestrial sources, not from algae in the lake. Nitrogen isotopic data suggest potential drying at the onset of the carbon isotope excursion, plus a potential trend toward greater cyanobacterial activity up section. Serial isotopic analysis of mussel shells support a shift from an environment where warm months are characterized by photosynthetic activity to one in which bacterial respiration dominates higher in the section, after the end of the CIE.

Acknowledgments

Cited Literature

Andreasson, F.P. & B. Schmitz. 1996. Winter and summer temperatures of the early middle Eocene of France from Turritella δ^{18}O profiles. – Geology 24: 1067-1070.

Bains, S., R.M. Corfield & R.D. Norris. 1999. Mechanisms of climate warming at the end of the Paleocene. – Science 285: 724-727.

Bains, S., R.D. Norris, R.M. Corfield, G.J. Bowen, P.D. Gingerich & P.L. Koch. 2003. Marine-terrestrial linkages at the Paleocene-Eocene boundary. In: Wing, S.L., P.D. Gingerich, B. Schmitz & E. Thomas. Eds. Causes and consequences of globally warm climates in the Early Paleogene. – Geological Society of America Special Paper 369: 1-9.

Bechtel, A., R. Gratzer, R.F. Sachsenhofer, J. Gusterhuber, A. Lücke, & W. Püttmann. 2008. Biomarker and carbon isotope variation in coal and fossil wood of Central Europe through the Cenozoic. – Palaeogeography, Palaeoclimatology, Palaeoecology 262: 166-175.

Bertrand, S., M. Sterken, L. Vargas-Ramirez, M. De Batist, W. Vyverman, G. Lepoint & N. Fagel. 2010. Bulk organic geochemistry of seidments from Puyehue Lake and its watershed (Chile, 40°S): Implications for paleoenvironmental reconstructions. – Palaeogeography, Palaeoclmatology, Palaeoecology 294: 56-71.

Bowen, G.J. & J.C. Zachos. 2010. Rapid carbon sequestration at the termination of the Palaeocene-Eocene thermal maximum. – Nature Geoscience 3: 866-869.

Brunet, F., K. Dubois, J. Viezer, G.R. Nkoue Ndondo, J.R. Ndam Ngoupayou, J.L. Boeglin, and J.L. Probst. 2009. Terrestrial and fluvial carbon fluxes in a tropical watershed: Nyong basin, Cameroon. – Chemical Geology 265: 563-572.

Carvajal-Ortiz, H., G. Mora & C. Jaramillo. 2009. A molecular evaluation of bulk organic carbon-isotope chemostratigraphy for terrestrial correlations: An example from two Paleocene-Eocene tropical sequences. – Palaeogeography, Palaeoclimatology, Palaeoecology 277: 173-183.

Choudhary P., J. Routh, and G.J. Chakrapani. 2009. An environmental record of changes in sedimentary organic matter from Lake Sattal in Kumaun Himalayas, India. – Science of the total environment 407: 2783-2795.

Clyde, W.C. & P.D. Gingerich. 1998. Mammalian community response to the latest Paleocene thermal maximum: An isotaphonomic study in the northern Bighorn Basin, Wyoming. – Geology 26: 1011-1014.

Clyde, W.C., J.A. Finarelli & K.E. Christensen. 2005. Evaluating the relationship between pedofacies and faunal composition: Implications for faunal turnover at the Paleocene-Eocene boundary. – Palaios 20: 390-399.

Coplen, T.B. 1994. Reporting of stable hydrogen, carbon, and oxygen isotopic abundances. Pure and applied chemistry 66: 273-276.

Dickens, G.R., J.R. O'Neil, D.K. Rea & R.M. Owen. 1995. Dissociation of oceanic methane hydrate as a cause of the carbon isotope excursion at the end of the Paleocene. – Paleoceanography 10: 965-971.

Dickens, G.R., M.M. Castillo &d J.C.G. Walker. 1997. A blast of gas in the latest Paleocene: Simulating first-order effects of massive dissociation of oceanic methane hydrate. – Geology 25: 259-262.

Dobbin, C.E., C.F. Bowen & H.W. Hoots. 1929. Geology and coal and oil resources of the Hanna and Carbon Basins, Carbon County, Wyoming. U.S. – Geological Survey Bulletin 804.

Dunn, R.E. 2003. Correlation of leaf megafossil and palynological data with North American land mammal ages from Paleocene-aged strata of the Ferris and Hanna formations, Hanna Basin, south-central Wyoming. – M.S. thesis, University of Wyoming, Laramie, Wyoming.

Fricke, H.C. & S.L. Wing. 2004. Oxygen isotope and paleobotanical estimates of temperature and δ^{18}O-latitude gradients over North America during the early Eocene. – American Journal of Science 304: 612-635.

Gillikin, D.P., A. Lorrain, S. Bouillon, P. Willenz & F. Dehairs. 2006. Stable carbon isotopic compositon of *Mytilus edulis* shells: relation to metabolism, salinity, δ^{13}CDIC and phytoplankton. – Organic Geochemistry 37: 1371-1382.

Gingerich, P.D. Ed. 2001. Paleocene-Eocene stratigraphy and biotic change in the Bighorn and Clarks Fork Basins, Wyoming. University of Michigan Papers on Paleontology 33.

Gingerich, P.D. 2003. Mammalian responses to climate change at the Paleocene-Eocene boundary: Polecat Bench record in the north-

ern Bighorn Basin, Wyoming. In: Wing, S.L., P.D. Gingerich, B. Schmitz & E. Thomas. Eds. Causes and consequences of globally warm climates in the Early Paleogene. – Geological Society of America Special Paper 369: 463-478.

Goodwin, D.H., B.R. Schöne & D.L. Dettman. 2003. Resolution and fidelity of oxygen isotopes as paleotemperature proxies in bivalve mollusk shells: Models and observations. – Palaios 18: 110-125.

Goodwin, D.H., K.W. Flessa, M.A. Téllez-Duarte, D.L. Dettman, B.R. Schöne & G.A. Avila-Serrano. 2004. Detecting time-averaging and spatial mixing using oxygen isotope variation: a case study. – Palaeogeography, Palaeoclimatology, Palaeoecology 205: 1-21.

Grossman, E.L., & T.-L. Ku. 1986. Oxygen and carbon isotope fractionation in biogenic aragonite: temperature effects. – Chemical Geology 59: 59-74.

Harrington, G.J. 2003. Geographic patterns in the floral response to Paleocene-Eocene warming. In: Wing, S.L., P.D. Gingerich, B. Schmitz & E. Thomas. Eds. Causes and consequences of globally warm climates in the Early Paleogene. – Geological Society of America Special Paper 369: 381-393.

Harrington, G.J. 2004. Structure of the North American vegetation gradient during the late Paleocene/early Eocene warm climate. – Evolutionary Ecology Research 6: 33-48.

Harrington, G.J., E.R. Clenchenko & D.C. Kelly. 2005. Palynology and organic-carbon isotope ratios across a terrestrial Palaeocene/Eocene boundary section in the Williston Basin, North Dakota, USA. – Palaeogeography, Palaeoclimatology, Palaeoecology 226: 214-232.

Higgins, P. 2003. A Wyoming succession of Paleocene mammal-bearing localitites bracketing the boundary between the Torrejonian and Tiffanian North American Land Mammal "Ages". Rocky Mountain Geology 38: 247-280.

Higgins, J.A. & D.P. Schrag. 2006. Beyond methane: Towards a theory for Paleocene-Eocene thermal maximum. – Earth and Planetary Science Letters 245: 523-537.

Ivany, L.C., B.H. Wilkinson, K.C. Lohmann, E.R. Johnson, B.J. McElroy & G.J. Cohen. 2004. Intra-annual isotopic variations in Venericardia bivalves: Implications for early Eocene

temperature, seasonality, and salinity on the U.S. Gulf Coast. – Journal of Sedimentary Research 74: 7-19.

Jones, D.S. & I.R. Quitmyer. 1996. Marking time with bivalve shells: oxygen isotopes and season of annual increment formation. – Palaios 11: 34-346.

Jones, D.S., I.R. Quitmyer & C.F.T. Andrus. 2005. Oxygen isotopic evidence for greater seasonality in Holocene shells of *Donax variabilis* from Florida. – Palaeogeography, Palaeoclimatology, Palaeoecology 228: 96-108.

Jones, M.D., M.J. Leng, W.J. Eastwood, D.H. Keen & C.S.M. Turney. 2002. Interpreting stable-isotope records from freshwater snail-shell carbonate: A Holocene case study from Lake Gölhisar, Turkey. – The Holocene 12: 629-634.

Jones, R.I., J. Grey, C. Quarmby & D. Sleep. 2001. Sources and fluxes of inorganic carbon in a deep, oligotrophic lake (Loch Ness, Scotland). – Global Biogeochemical Cycles 15: 863-870.

Kennett, J.P. & L.D. Stott. 1991. Abrupt deep sea warming, paleoceanographic changes and benthic extinctions at the end of the Palaeocene. – Nature 353: 319-322.

Kirschner, W.A. 1984. Nonmarine molluscan paleontology and paleoecology of early Tertiary strata, Hanna Basin, Wyoming. – M.S. thesis, University of Wyoming, Laramie, Wyoming.

Koch, P.L., J.C. Zachos & P.D. Gingerich. 1992. Correlation between isotope records in marine and continental carbon reservoirs near the Palaeocene/Eocene boundary. – Nature 358: 319-322.

Koch, P.L., J.C. Zachos & D.L. Dettman. 1995. Stable isotope stratigraphy and paleoclimatology of the Paleogene Bighorn Basin (Wyoming, USA). – Palaeogeography, Palaeoclimatology, Palaeoecology 115: 61-89.

Koch, P.L., W.C. Clyde, R.P. Hepple, M.L. Fogel, S.L. Wing & J.C. Zachos. 2003. Carbon and oxygen isotope records from paleosols spanning the Paleocene-Eocene boundary, Bighorn Basin, Wyoming. In: Wing, S.L., P.D. Gingerich, B. Schmitz & E. Thomas. Eds. Causes and consequences of globally warm climates in the Early Paleogene. – Geological Society of America Special Paper 369: 49-64.

Kraus, M.J. & S. Riggins. 2007. Transient drying during the Paleocene-Eocene Thermal

Maximum (PETM): Analysis of paleosols in the Bighorn Basin, Wyoming. – Palaeogeography, Palaeoclimatology, Palaeoecology 245: 444-461.

Kvenvolden, K.A. 1999. Potential effects of gas hydrate on human welfare. – Proceedings of the National Academy of Sciences 96: 3420-3426.

Lillegraven, J.A. & J.J. Eberle. 1999. Vertebrate faunal changes through Lancian and Puercan time in southern Wyoming. – Journal of Paleontology 73: 689-708.

Lillegraven, J.A. & A.W. Snoke. 1996. A new look at the Laramide orogeny in the Seminoe and Shirley Mountains, Freezeout Hills, and Hanna Basin, south-central Wyoming. – Wyoming State Geological Survey, Public Information Circular 36.

Lillegraven, J.A., A.W. Snoke & M.C. McKenna. 2004. Tectonic and paleogeographic implications of late Laramide geologic history in the northeastern corner of Wyoming's Hanna Basin. – Rocky Mountain Geology 39: 7-64.

Magioncalda, R., C. Dupuis, T. Smith, E. Steurbaut & P.D. Gingerich. 2004. Paleocene-Eocene carbon isotope excursion in organic carbon and pedogenic carbonate: Direct comparison in a continental stratigraphic section. – Geology 32: 553-556.

McConnaughey, T.A. 2003. Sub-equilibrium oxygen-18 and carbon-13 levels in biological carbonates: Carbonate and kinetic models. – Coral Reefs 22: 316-327.

McConnaughey, T.A. & D.P. Gillikin. 2008. Carbon isotopes in mollusk shell carbonates. – Geo-Marine Letters 28: 287-299.

McConnaughey, T.A., J. Burdett, J.F. Whelan & C.K. Paull. 1997. Carbon isotopes in biological carbonates: respiration and photosynthesis. – Geochimica et Cosmochimica Acta 61: 611-622.

Meyers, P.A. 1997. Organic and geochemical proxies of paleoceanographic, paleolimnologic, and paleoclimatic processes. – Organic Geochemistry 27: 213-250.

Meyers, P.A. & R. Ishiwatari. 1993. Lacustrine organic geochemistry—an overview of indicators of organic matter sources and diagenesis in lake sediments. – Organic Geochemistry 20: 867-900.

Röhl, U., T.J. Bralower, R.D. Norris & G. Wefer. 2000. New chronology for the late Paleocene thermal maximum and its environmental implications. – Geology 28: 927-930.

Röhl, U., T. Westerhold, T.J. Bralower & J.C. Zachos. 2007. On the duration of the Paleocene-Eocene thermal maximum (PETM). – Geochemistry Geophysics Geosystems 8 (Q12002, doi:10.1029/2007GC001784).

Romanek, C.S. & E.L. Grossman. 1989. Stable isotope profiles of Tridacna maxima as environmental indicators. – Palaios 4: 402-413.

Routh, J., P.A. Meyers, Ö. Gustafsson, M. Baskaran, R. Hallberg & A. Schöldström. 2004. Sedimentary geochemical record of human-induced environmental changes in the Lake Brunnsviken watershed, Sweden. – Limnology and Oceanography 49: 1560-1569.

Schmitz, B. & F.P. Andreasson. 2001. Air humidity and lake $\delta^{18}O$ during the latest Paleocene earliest Eocene in France from recent and fossil fresh-water and marine gastropod $\delta^{18}O$, $\delta^{13}C$, and 87Sr/86Sr. – Geological Society of America Bulletin 113: 774-789.

Schöne, B.R., D.L. Rodland, J. Fiebig, W. Oschmann, D. Goodwin, K.W. Flessa & D. Dettman. 2006. Reliability of multitaxon, multiproxy reconstructions of environmental conditions from accretionary biogenic skeletons. – Journal of Geology 114: 267-285.

Schouten, S., M. Woltering, W.I.C. Rijpstar, A. Sluijs, H. Brinkhuis & J.S.S. Damste. 2007. The Paleocene-Eocene carbon isotope excursion in higher plant organic matter: Differential fractionation of angiosperms and conifers in the Arctic. – Earth and Planetary Science Letters 258: 581-592.

Smith, F.A., S.L. Wing & K.H. Freeman. 2007. Magnitude of the carbon isotope excursion at the Paleocene-Eocene thermal maximum: The role of plant community change. – Earth and Planetary Science Letters 262: 50-65.

Vagenas, N.V., A. Gatsouli & C.G. Kontoyannis. 2003. Quantitative analysis of synthetic calcium carbonate polymorphs using FT-IR spectroscopy. – Talanta 59: 831-836.

Veinott, G.I. & R.J. Cornett. 1998. Carbon isotopic disequilibrium in the shell of the freshweater mussel *Elliptio complanata*. – Applied Geochemistry 13: 4957.

Wing, S.L., G.J. Harrington, G.J. Bowen & P.L. Koch. 2003. Floral change during the Initial Eocene Thermal Maximum in the Powder River Basin, Wyoming. In: Wing, S.L., P.D. Gingerich, B. Schmitz & E. Thomas. Eds. Causes and consequences of globally warm

climates in the Early Paleogene. – Geological Society of America Special Paper 369: 425-440.

Yamamuro, M. & Y. Kanai. 2005. A 200-year record of natural and anthropogenic changes in water quality from coastal lagoon sediments of Lake Shinji, Japan. – Chemical Geology 218: 51-61.

Yans, J., S.G. Strait, T. Smith, C. Dupuis, E. Steurbaut & P.D. Gingerich. 2006. High-resolution carbon isotope stratigraphy and mammalian faunal change at the Paleocene-Eocene boundary in the Honeycombs area of the southern Bighorn Basin, Wyoming. – American Journal of Science 306: 712-735.

Zachos, J.C., K.C. Lohmann, J.C. Walker & S.W. Wise. 1993. Abrupt climate change and transient climates during the Paleogene: A marine perspective. – Journal of Geology 101: 191-213.

Submitted: 30 January 2011
Published 5 April 2012

ICZN
To comply with Article 8.6 of the International Code of Zoological Nomenclature (4th edition), this journal is deposited as hard copy in four archival libraries and the archive of the PalArch Foundation. All of PalArch's publications are stored in the e-depot of The National Library, The Hague, The Netherlands (www.kb.nl).

Natural History Museum Rotterdam
Westzeedijk 345
3015 AA Rotterdam
The Netherlands

Royal Belgian Institute of Natural Sciences
Library
rue Vautier 29
B- 1000 Brussels
Belgium

Library Naturalis
National Museum of Natural History
P.O. Box 9517
2300 RA Leiden
The Netherlands

PalArch Foundation
Mezquitalaan 23
1064 NS Amsterdam
The Netherlands

Vrije Universiteit
UBVU-Library of Earth Sciences
De Boelelaan 1079
1081 HV Amsterdam
The Netherlands

OurLabID	Sample ID	Carbon	Oxygen	Serial Position	Stratigraphic level
C-2451	JVTB08-01	-0.9	-7.8	6.8	2757
C-2452	JVTB08-02	-1.5	-9.2	9.8	2757
C-2453	JVTB08-03	-0.5	-7.9	11.4	2757
C-2472	JVTB08-22	0.6	-6.8	11.4	2757
C-2473	JVTB08-23	-1.2	-8.5	13.0	2757
C-2454	JVTB08-04	-2.9	-12.7	13.8	2757
C-2474	JVTB08-24	-0.5	-6.5	15.0	2757
C-2455	JVTB08-05	-2.3	-12.4	15.2	2757
C-2456	JVTB08-06	-1.4	-10.3	16.9	2757
C-2476	JVTB08-26	-2.0	-12.2	17.5	2757
C-2457	JVTB08-07	-1.4	-9.3	18.0	2757
C-2458	JVTB08-08	-2.0	-8.9	18.7	2757
C-2459	JVTB08-09	-1.1	-8.2	20.4	2757
C-2460	JVTB08-10	-1.2	-7.6	21.4	2757
C-2461	JVTB08-11	-1.5	-6.5	22.8	2757
C-2462	JVTB08-12	-0.2	-4.8	24.0	2757
C-2479	JVTB08-29	1.2	-6.3	24.0	2757
C-2463	JVTB08-13	0.5	-5.4	25.3	2757
C-2480	JVTB08-30	-1.2	-9.7	25.8	2757
C-2464	JVTB08-14	-1.8	-9.4	27.1	2757
C-2482	JVTB08-32	-2.4	-12.3	28.5	2757
C-2465	JVTB08-15	-2.8	-11.1	28.6	2757
C-2466	JVTB08-16	-3.0	-10.4	29.2	2757
C-2484	JVTB08-34	-2.5	-10.0	31.1	2757
C-2467	JVTB08-17	-3.0	-10.5	31.2	2757
C-2486	JVTB08-36	-0.3	-8.1	32.8	2757
C-2468	JVTB08-18	-0.2	-8.8	33.8	2757
C-2469	JVTB08-19	-0.2	-7.5	36.0	2757
C-2470	JVTB08-20	-1.5	-9.1	37.6	2757
C-3912	JM-TB-10-24	-0.5	-12.4	2.6	2710
C-3913	JM-TB-10-25	-1.2	-11.2	4.1	2710
C-3890	JM-TB-10-02	-4.0	-13.0	5.0	2710
C-3914	JM-TB-10-26	-0.9	-12.2	5.8	2710
C-3891	JM-TB-10-03	-4.7	-15.2	6.4	2710
C-3892	JM-TB-10-04	-4.1	-13.6	7.4	2710
C-3916	JM-TB-10-28	-0.4	-10.8	8.2	2710
C-3917	JM-TB-10-29	-0.1	-11.6	8.8	2710
C-3894	JM-TB-10-06	-4.1	-17.6	10.1	2710
C-3918	JM-TB-10-30	0.4	-11.9	10.3	2710
C-3919	JM-TB-10-31	-0.4	-11.9	11.4	2710
C-3895	JM-TB-10-07	-4.4	-16.2	11.6	2710
C-4000	JM-TB-10-54	-0.4	-6.2	12.5	2710
C-4000	JM-TB-10-54	-0.5	-6.1	12.5	2710
C-3896	JM-TB-10-08	-3.8	-14.6	12.5	2710
C-3920	JM-TB-10-32	-0.4	-10.9	13.0	2710

OurLabID	Sample ID	Carbon	Oxygen	Serial Position	Stratigraphic level
C-3897	JM-TB-10-09	-3.6	-10.7	13.6	2710
C-4003	JM-TB-10-57	0.2	-4.8	14.2	2710
C-4004	JM-TB-10-58	0.0	-6.0	14.6	2710
C-3898	JM-TB-10-10	-2.6	-9.1	15.0	2710
C-3899	JM-TB-10-11	-1.7	-8.4	15.9	2710
C-3900	JM-TB-10-12	-1.0	-8.8	16.6	2710
C-4009	JM-TB-10-63	1.2	-6.4	17.6	2710
C-4009	JM-TB-10-63	1.0	-6.6	17.6	2710
C-3901	JM-TB-10-13	-0.8	-11.1	18.5	2710
C-3902	JM-TB-10-14	-1.7	-11.5	19.4	2710
C-4012	JM-TB-10-66	-0.5	-6.2	19.5	2710
C-4013	JM-TB-10-67	-0.2	-6.5	20.3	2710
C-3903	JM-TB-10-15	-4.2	-16.1	20.9	2710
C-4015	JM-TB-10-69	0.3	-6.2	21.7	2710
C-3904	JM-TB-10-16	-4.1	-16.3	21.7	2710
C-3905	JM-TB-10-17	-3.7	-10.6	22.7	2710
C-4018	JM-TB-10-72	-1.1	-7.5	23.8	2710
C-3906	JM-TB-10-18	-4.7	-13.4	23.9	2710
C-4019	JM-TB-10-73	-0.9	-6.4	24.6	2710
C-3908	JM-TB-10-20	-5.0	-14.8	25.8	2710
C-3909	JM-TB-10-21	-5.2	-13.7	26.4	2710
C-3910	JM-TB-10-22	-5.4	-10.4	27.8	2710
C-4024	JM-TB-10-78	-0.5	-7.1	28.3	2710
C-4024	JM-TB-10-78	-0.4	-7.4	28.3	2710
C-4028	JM-TB-10-82	-1.3	-7.8	31.6	2710
C-4031	JM-TB-10-85	-0.5	-7.5	33.9	2710
C-4032	JM-TB-10-86	-0.3	-7.4	34.1	2710
C-4036	JM-TB-10-90	-0.3	-6.9	36.7	2710
C-4037	JM-TB-10-91	-0.4	-6.9	37.4	2710
C-4040	JM-TB-10-94	0.2	-7.5	39.1	2710
C-4041	JM-TB-10-95	-0.4	-7.5	40.3	2710
C-2487	JVTB08-37	-2.2	-13.5	8.6	2632
C-2488	JVTB08-38	-4.8	-13.6	9.8	2632
C-2489	JVTB08-39	-5.4	-13.7	10.5	2632
C-2490	JVTB08-40	-5.0	-11.6	11.2	2632
C-2491	JVTB08-41	-3.7	-10.4	11.9	2632
C-2492	JVTB08-42	-2.4	-10.4	12.8	2632
C-2493	JVTB08-43	-2.5	-11.3	13.6	2632
C-2494	JVTB08-44	-3.9	-12.7	14.1	2632
C-2495	JVTB08-45	-5.1	-13.1	14.7	2632
C-2496	JVTB08-46	-5.3	-13.0	16.2	2632
C-2660	SIR 08-39	-0.7	-4.8	1.0	2235
C-2661	SIR 08-40	-1.5	-5.1	2.0	2235
C-2662	SIR 08-41	-2.2	-6.2	3.0	2235
C-2663	SIR 08-42	-2.4	-5.1	4.0	2235

OurLabID	Sample ID	Carbon	Oxygen	Serial Position	Stratigraphic level
C-2664	SIR 08-43	-2.6	-5.4	5.0	2235
C-2665	SIR 08-44	-2.4	-5.3	6.0	2235
C-2666	SIR 08-45	-2.4	-4.3	7.0	2235
C-2667	SIR 08-46	-1.8	-4.8	8.0	2235
C-2668	SIR 08-47	-2.5	-4.1	9.0	2235
C-2669	SIR 08-48	-2.1	-3.7	10.0	2235
C-2670	SIR 08-49	-1.4	-6.3	11.0	2235
C-2671	SIR 08-50	-1.2	-6.6	12.0	2235
C-2672	SIR 08-51	-4.2	-11.7	1.0	2210
C-2673	SIR 08-52	-3.4	-12.7	2.0	2210
C-2674	SIR 08-53	-3.5	-11.5	3.0	2210
C-2676	SIR 08-55	-4.7	-12.1	5.0	2210
C-2677	SIR 08-56	-4.3	-11.8	6.0	2210
C-2678	SIR 08-57	-4.7	-12.8	7.0	2210

Appendix I. All individual data points from the eight mussel shells sampled in this study.